Layer-specific fiber distribution in arterial tissue modeled as a constrained mixture

Klaas Vander Linden[a*], Milad Ghasemi[a], Lauranne Maes[a], Julie Vastmans[a], Nele Famaey[a]

[a] *Biomechanics Section, Mechanical Engineering Department, KU Leuven, Leuven, Belgium*

Abstract

Collagen fibers and their orientation greatly influence an artery's mechanical characteristics, determining its transversely isotropic behavior. It is generally assumed that these fibers are deposited along a preferred direction to maximize the load bearing capacity of the vessel wall. This implies a large spatial variation in collagen orientation which can be reconstructed in numerical models using so-called reorientation algorithms. Until now, these algorithms have used the classical continuum mechanics modeling framework which requires knowledge of tissue-level parameters and the artery's stress-free reference state, which is inaccessible in a clinical context. We present an algorithm to compute the preferred fiber distribution compatible with the constrained mixture theory, which orients two collagen fiber families according to the loading experienced by the isotropic non-collagenous extracellular matrix, without requiring prior knowledge of the stress-free state. Because consensus is lacking whether stress or stretch is the determining factor behind the preferred fiber distribution, we implemented both approaches and compared the results with experimental microstructural data of an abdominal aorta. The stress-based algorithm was able to describe several experimentally observed transitions of the fiber distribution across the intima, media and adventitia.

Keywords: collagen fiber distribution, constrained mixture theory, arterial

*Corresponding author: K. Vander Linden, KU Leuven, Biomechanics Section, Celestijnenlaan 300C, 3001 Heverlee (Belgium)

Email address: klaas.vanderlinden@kuleuven.be (Klaas Vander Linden[a])

1. Introduction

Like many other types of biological tissue, arteries have the ability to adapt to changes in their mechanobiological environment. Cells are able to alter the extracellular matrix (ECM) by synthesizing new constituents or by secreting matrix enhancing or degrading products [1]. Out of the various ECM constituents, prior studies focused mainly on the collagen fibers because of their important load bearing capacity, whereby their orientation defines the artery's transversely isotropic behavior. It has been hypothesized that cells sense their mechanical environment and deposit the new fibers along a preferred direction to maximize the load bearing capacity of the vessel wall [1]. Numerical models can be used to calculate these directions of principal stresses and strains, and consequently predict the fiber alignment throughout the arterial wall according to a certain hypothesis. Driessen *et al.* first proposed a computational model which aligned the fibers with the principal stretch directions [2]. Although promising results were obtained for the fiber alignment in heart valves, the typical helical structure found in arteries could not be predicted. An adjusted model aligned the collagen fibers in between the first and second principal stretch directions [3]. The hammock-like fiber structure in heart valves could be retrieved [4], as well as the collagen architecture found in articular cartilage [5]. Additionally, the angular fiber distribution around the preferred fiber direction was also subjected to remodeling rules in an extended version of this model [6]. According to Taber and Humphrey, stress and not strain is the driving force behind growth an remodeling in arteries [7]. Therefore, Hariton *et al.* proposed a model realigning the collagen fibers in between the first and second principal stress directions [8] and applied it on carotid bifurcations [9]. Besides these stretch- or stress-based reorientation rules, others have implemented alternative laws based on *e.g.* virtual energy [10], membrane theory [11] or on the minimization of the total potential energy [12].

The constrained mixture theory was first described by Humphrey and Rajagopal and describes the stress state of different constituents in an *in vivo* reference state using a constituent-specific deposition stretch with respect to their individual, stress-free states [13]. Despite its continuum-level approach,

the biofidelic assumptions with respect to the underlying microstructure render it an effective basis for various growth and remodeling frameworks and allows to account for different production and degradation processes while considering the different stresses experienced by the different constituents. Moreover, the constrained mixture theory allows to model the residual stresses in patient specific arteries without the need of identifying the clinically inaccessible opened, stress-free configuration [14].

Despite the microstructural motivation behind the aforementioned models, collagen fiber distribution has not yet been studied within the framework of the constrained mixture theory. Different studies superimposed the effect of residual stress after finding the optimal fiber orientation [12, 15, 16], but did not model both phenomena simultaneously.

Fibroblasts and synthetic smooth muscle cells which are assumed to be embedded in the non-collagenous, quasi-isotropic part of the ECM are responsible for synthesizing the collagen fibers [1, 17]. In the present study, we introduce an algorithm which determines the fiber distribution according to the loading experienced by this non-collagenous ECM based on the constrained mixture theory. Because consensus is lacking in literature, we implemented both a stress- and stretch-based fiber distribution. As a first validation, we compared the results of both methods to experimental microstructural data from literature.

The work is structured as follows. Section 2 describes the constrained mixture based constitutive model, the fiber distribution laws and their numerical implementation. The results of the methods applied to an idealized abdominal aorta are shown in Section 3, which are further discussed in Section 4. Finally, Section 5 summarizes the most important conclusions.

2. Materials and Methods

2.1. Constrained mixture compatible material description

Arterial tissue can be described as a fiber-reinforced, incompressible, transversely isotropic material as proposed by Gasser *et al.* [18]. It is assumed to be composed of an isotropic hyperelastic non-collagenous ECM, and two symmetrically oriented collagen fiber families. The total strain energy of the mixture additively decomposes to:

$$\Psi = \Psi^{(\mathrm{e})}(\mathbf{C}^{(\mathrm{e})}) + \Psi^{(\mathrm{c})}(\mathbf{C}^{(\mathrm{c})}, \mathbf{M}_{i,0}) - p(J-1), \quad i = 4, 6, \tag{1}$$

assuming incompressibility ($J = \det(\mathbf{F}) = 1$) and with $\mathbf{C}^{(\mathrm{e})}$ and $\mathbf{C}^{(\mathrm{c})}$ the right Cauchy Green tensors of the isotropic matrix and collagen, respectively. $\mathbf{M}_{i,0}$ represents the main fiber direction of collagen family i in the reference configuration. The non-collagenous ECM, mainly consisting of elastin, is modeled using a Neo-Hookean material model:

$$\Psi^{(\mathrm{e})} = C_{10}(I_1^{(\mathrm{e})} - 3), \tag{2}$$

where $I_1^{(\mathrm{e})}$ is the first invariant of $\mathbf{C}^{(\mathrm{e})}$ and C_{10} is a stress-like material parameter representing the matrix' stiffness.
The collagen fibers' contribution to the total strain energy function is considered to be:

$$\Psi^{(\mathrm{c})} = \frac{k_1}{2k_2} \sum_{i=4,6} \{\exp(k_2[(\kappa I_1^{(\mathrm{c})} + (1 - 3\kappa_{0,k}) I_i^{(\mathrm{c})}) - 1]^2) - 1\}, \tag{3}$$

$$I_i^{(\mathrm{c})} = \mathbf{C}^{(\mathrm{c})} : \mathbf{M}_{i,0} \otimes \mathbf{M}_{i,0}, \quad i = 4, 6, \tag{4}$$

with $I_1^{(\mathrm{c})}$ the first invariant of $\mathbf{C}^{(\mathrm{c})}$ and $I_i^{(c)}$ the pseudo invariants of $\mathbf{C}^{(\mathrm{c})}$ representing the stretch along the main fiber direction $\mathbf{M}_{i,0}$. k_1, k_2 and $\kappa_{0,k}$ represent the fiber stiffness, fiber stiffening and preferred fiber dispersion, respectively.
According to the constrained mixture theory, different arterial constituents are related to an individual stress-free state which is related to the *in vivo* homeostatic reference state by a constituent-specific depostion stretch tensor [19]. The constituent-specific right Cauchy Green tensor is defined as

$$\mathbf{C}^{(j)} = {\mathbf{F}^{(j)}}^T \mathbf{F}^{(j)}, \quad \text{with} \quad \mathbf{F}^{(j)} = \mathbf{F}\mathbf{G}^{(j)} \quad \text{and} \quad j = e, c, \tag{5}$$

with $\mathbf{F}$ the total deformation gradient of the mixture with respect to the *in vivo* reference configuration and $\mathbf{G}^{(j)}$ the prestretch at which constituent j is deposited [19]. Similar to other studies in which the constrained mixture theory has been adopted [20, 21], the diastolic configuration is assumed to be the reference configuration.
The second Piola-Kirchhoff and Cauchy stress tensor are calculated as

$$\mathbf{S}^{(j)} = 2\frac{\partial \Psi^{(\mathrm{j})}}{\partial \mathbf{C}} \tag{6}$$

and

$$\boldsymbol{\sigma}^{(j)} = \det(\mathbf{F})^{-1}\mathbf{F}\mathbf{S}^{(j)}\mathbf{F}, \tag{7}$$

respectively.
Collagen, having a high turn-over rate, has a deposition stretch $g^{(c)}$ in the preferred direction of its fibers, which can be assumed to be independent of the homeostatic state in matured arteries. The collagen-specific prestretch of fiber family i is therefore defined as [22]

$$\mathbf{G}_i^{(c)} = g^{(c)}\mathbf{M}_{i,0} \otimes \mathbf{M}_{i,0} + \frac{1}{\sqrt{g^{(c)}}}(\mathbf{I} - \mathbf{M}_{i,0} \otimes \mathbf{M}_{i,0}), \quad i = 4, 6, \tag{8}$$

with $\mathbf{I}$ the identity tensor.
In contrast to collagen, elastin is produced during perinatal development and remains relatively stable thereafter. This implies that in a matured artery, the elastin underwent complex, multi-axial deformation which varies throughout the tissue. The deposition stretch of the non-collagenous ECM $\mathbf{G}^{(e)}$ can be determined assuming isochoric deformation and static equilibrium in the *in vivo* reference configuration which is experiencing a known luminal pressure [20, 23]. The axial component of $\mathbf{G}^{(e)}$ is assumed to be known.

2.2. Constrained-mixture based fiber distribution

In this study, we propose a stress- and stretch-modulated fiber distribution algorithm embedded in the constrained mixture theory. We hypothesize that collagen fiber distribution is driven by either the tensile stresses or stretches experienced by the non-collagenous ECM. We thereby consider a constant collagen fiber type, content and deposition stretch $g^{(c)}$ throughout the wall

layer.
The main collagen fiber direction $\mathbf{M}_{i,0}$ is expressed in a coordinate system defined by the directions of either the principal stress ($k = \sigma$) or principal stretch ($k = \lambda$) experienced by the non-collagenous ECM:

$$\begin{aligned} \mathbf{M}_{4,0} &= \cos\gamma_{0,k}\mathbf{e}^{(e)}_{1,k} + \sin\gamma_{0,k}\mathbf{e}^{(e)}_{2,k}, \\ \mathbf{M}_{6,0} &= \cos\gamma_{0,k}\mathbf{e}^{(e)}_{1,k} - \sin\gamma_{0,k}\mathbf{e}^{(e)}_{2,k}, \end{aligned} \tag{9}$$

with $\mathbf{e}^{(e)}_{1,\sigma}$ and $\mathbf{e}^{(e)}_{2,\sigma}$ the unit vectors defining the first and second principal direction of $\boldsymbol{\sigma}^{(e)}|_{\mathbf{F}=\mathbf{I}}$, respectively, and $\mathbf{e}^{(e)}_{1,\lambda}$ and $\mathbf{e}^{(e)}_{2,\lambda}$ the unit vectors defining the first and second principal direction of $\mathbf{C}^{(e)}|_{\mathbf{F}=\mathbf{I}}$, respectively. $\gamma_{0,k}$ is defined as the preferred main fiber angle with respect to $\mathbf{e}^{(e)}_{1,k}$ ($k = \sigma, \lambda$), assuming both fiber families are symmetrically oriented with respect to $\mathbf{e}^{(e)}_{1,k}$. The preferred main fiber angle is defined by the ratio of two stimulus functions $s_{1,k}$ and $s_{2,k}$:

$$\gamma_{0,k} = \arctan\left(\frac{s_{2,k}}{s_{1,k}}\right). \tag{10}$$

Similar to Driessen *et al.* who related the angular fiber distribution to the ratio of the two maximal principal stretch directions [6], we assume that $\kappa_{0,k}$, used to characterize the distribution around the preferred angle, is governed by the ratio of the two stimulus functions:

$$\kappa_{0,k} = \frac{1}{3}\frac{s_{2,k}}{s_{1,k}}. \tag{11}$$

Depending on the adopted method, which can be either stress- or stretch-based, the stimulus functions are specified as follows (with $i = 1, 2$):

$$s_{i,k} = \begin{cases} \sigma^{(e)}_i|_{\mathbf{F}=\mathbf{I}} = \mathbf{e}^{(e)}_{i,\sigma} \cdot \boldsymbol{\sigma}^{(e)}|_{\mathbf{F}=\mathbf{I}} \cdot \mathbf{e}^{(e)}_{i,\sigma} & \text{if} \quad k = \sigma, \\ \lambda^{(e)}_i|_{\mathbf{F}=\mathbf{I}} = \sqrt{\mathbf{e}^{(e)}_{i,\lambda} \cdot \mathbf{C}^{(e)}|_{\mathbf{F}=\mathbf{I}} \cdot \mathbf{e}^{(e)}_{i,\lambda}} & \text{if} \quad k = \lambda, \end{cases} \tag{12}$$

with $\sigma^{(e)}_1|_{\mathbf{F}=\mathbf{I}}$ and $\sigma^{(e)}_2|_{\mathbf{F}=\mathbf{I}}$ the first and second principal Cauchy stress component and $\lambda^{(e)}_1|_{\mathbf{F}=\mathbf{I}}$ and $\lambda^{(e)}_2|_{\mathbf{F}=\mathbf{I}}$ the first and second principal stretch component experienced by the non-collagenous ECM in the reference configuration.

2.3. Numerical implementation

This section combines Sections 2.1 and 2.2 and describes an analytical procedure to calculate the deposition stretches and corresponding collagen fiber distribution throughout the arterial wall layers of a healthy human abdominal aorta.

2.3.1. Calculating deposition stretches and fiber distribution

To estimate the transmural collagen fiber distribution, the aorta is approached as an axisymmetric thick-walled cylinder with an inner radius R_{inner} corresponding to a diastolic pressure P_{dias}. For this regular geometry, the circumferential ($\mathbf{e}_{\Theta\Theta}$), axial ($\mathbf{e}_{ZZ}$) and radial ($\mathbf{e}_{RR}$) axes are well-defined. Hence, the deformation gradient with respect to the diastolic reference state after extension and inflation using the incompressibility constraint is given as

$$\mathbf{F} = \begin{bmatrix} \frac{1}{\lambda_{\theta\theta}\lambda_{zz}} & 0 & 0 \\ 0 & \lambda_{\theta\theta} & 0 \\ 0 & 0 & \lambda_{zz} \end{bmatrix} \tag{13}$$

with $\lambda_{\theta\theta}$ and λ_{zz} the circumferential and axial stretch, respectively. $\lambda_{zz} = l/L$, with L and l the reference and deformed axial length, respectively. $\lambda_{\theta\theta} = r/R$, with R and r the radial position in the reference and deformed configuration respectively. Ensuring that the cylindrical shape is preserved during the extension-inflation with no volume change, we derive an expression of $\lambda_{\theta\theta}$ throughout the wall for a given $\lambda_{\theta\theta,inner} = r_{inner}/R_{inner}$ [24]:

$$\begin{aligned} V &= v \\ &\Updownarrow \\ L\pi(R^2 - R_{inner}^2) &= l\pi(r^2 - r_{inner}^2) \\ &\Downarrow \\ \lambda_{\theta\theta} = \frac{r}{R} &= \frac{\sqrt{\left(\lambda_{\theta\theta,inner} R_{inner}\right)^2 + \frac{R^2 - R_{inner}^2}{\lambda_{zz}}}}{R}, \end{aligned} \tag{14}$$

with V and v the cylindrical wall volume in the reference and deformed state.

From the force equilibrium of a thick-walled cylinder, a relationship between

luminal pressure P and intramural stress is obtained [24]:

$$P = \int_{r_{inner}}^{r_{outer}} \frac{\sigma_{\theta\theta} - \sigma_{rr}}{r} dr, \tag{15}$$

with $\sigma_{\theta\theta}$ and σ_{rr} the circumferential and radial component of the total intramural stress tensor $\boldsymbol{\sigma}$ at radial position r.
The deposition stretches $\mathbf{G}^{(e)}$ and $\mathbf{G}^{(c)}_{4,6}$ should enable static equilibrium of the *in vivo* geometry experiencing the internal pressure measured at the reference state, *i.e.* $\mathbf{F} = \mathbf{I}$ throughout the entire wall. $\mathbf{G}^{(e)}$ is assumed to characterize an extension-inflation between the stress-free state and the reference state:

$$\mathbf{G}^{(e)} = \begin{bmatrix} \frac{1}{g^{(e)}_{\Theta\Theta} g^{(e)}_{ZZ}} & 0 & 0 \\ 0 & g^{(e)}_{\Theta\Theta} & 0 \\ 0 & 0 & g^{(e)}_{ZZ} \end{bmatrix} \tag{16}$$

with $g^{(e)}_{\Theta\Theta}$ and $g^{(e)}_{ZZ}$ the circumferential and axial deposition stretch of the isotropic non-collagenous ECM, respectively. $g^{(e)}_{\Theta\Theta}$ is dependent on the radial position and defined as R/r_0, with r_0 the radial position in the stress-free configuration. It has been hypothesized that $\mathbf{G}^{(e)}$ originates from developmental stretches [14]. Therefore, similar to equation 14, the distribution of $g^{(e)}_{\Theta\Theta}$ throughout the wall can be described as

$$g^{(e)}_{\Theta\Theta} = \frac{R}{\sqrt{\left(\frac{R_{inner}}{g^{(e)}_{\Theta\Theta,inner}}\right)^2 + g^{(e)}_{ZZ}(R^2 - R^2_{inner})}}. \tag{17}$$

For a known $g^{(e)}_{\Theta\Theta,inner}$ and $g^{(e)}_{ZZ}$, the corresponding stress- or stretch-driven transmural fiber distribution is determined using the equations stated in Section 2.2.

To compare with experimental data, which is typically measured on excised samples, we need to derive the fiber distribution in the stress-free state. Therefore, after finding the deposition stretches and collagen fiber distribution in the homeostatic reference state, $\mathbf{F}_{\text{rel}} = diag(\frac{1}{\lambda_{\theta\theta,rel}\lambda_{zz,rel}}, \lambda_{\theta\theta,rel}, \lambda_{zz,rel})$ is defined as the deformation gradient yielding an internal pressure P of

0mmHg (see equation 15) and axial force N of 0N, which is defined as [24]:

$$N = 2\pi \int_{r_{inner}}^{r_{outer}} \sigma_{zz} r dr. \tag{18}$$

This state is fully determined using equation 14.
$\mathbf{F}_{\text{rel}}$ is then used to derive the preferred fiber direction in the stress-free state:

$$\mathbf{m}_{i,\text{rel}} = \frac{\mathbf{F}_{\text{rel}}\mathbf{M}_{i,0}}{|\mathbf{F}_{\text{rel}}\mathbf{M}_{i,0}|}, \quad i = 4, 6. \tag{19}$$

To compare with the experimental data reported in [25], we defined $\alpha_{0,k,i}$ and $\alpha_{rel,k,i}$, the positive angles between the preferred direction of fiber family i in its respective state and the circumferential direction of the artery. For an idealized cylinder with symmetrically oriented fiber families, the direction of the maximal principal stress $\mathbf{e}_{1,\sigma}$ and stretch $\mathbf{e}_{1,\lambda}$ coincides with either the axial or circumferential axis, such that both fiber families can be described by a single fiber angle for each state:

$$\alpha_{0,k} = \alpha_{0,k,i} = |\angle(\mathbf{M}_{i,0}, \mathbf{e}_{\Theta\Theta})|, \tag{20}$$

$$\alpha_{rel,k} = \alpha_{rel,k,i} = \left|\angle\left(\mathbf{m}_{i,rel}, \frac{\mathbf{F}_{\text{rel}}\mathbf{e}_{\Theta\Theta}}{|\mathbf{F}_{\text{rel}}\mathbf{e}_{\Theta\Theta}|}\right)\right|, \tag{21}$$

with $k = \sigma, \lambda$ and $i = 4$ or 6.
The collagen density $\rho(\phi)$ in the stress-free state corresponding to the preferred fiber directions and dispersion is calculated according to a π-periodic *Von Mises* distribution, following [18]:

$$\rho(\phi) = \frac{2}{a}\sqrt{\frac{b}{2\pi}}\Big[\exp[b(\cos(2(\phi + \alpha_{rel,k})) + 1)] + \exp[b(\cos(2(\phi - \alpha_{rel,k})) + 1)]\Big], \tag{22}$$

with ϕ ($-\frac{\pi}{2} < \phi < \frac{\pi}{2}$) the fiber angle with respect to the circumferential direction and $b > 0$ the concentration parameter directly related to $\kappa_{rel,k} = \kappa_{0,k}$, with $k = \sigma, \lambda$. For further details on this relationship, see [18]. The normalized fiber density is further calculated as $\overline{\rho}(\phi) = \frac{\rho(\phi)}{\max\limits_{-\frac{\pi}{2}<\phi<\frac{\pi}{2}} \rho(\phi)}$.

2.3.2. Application on a human healthy abdominal aorta

Previously, Niestrawska *et al.* experimentally examined the collagen fiber microstructure of healthy human abdominal aortic tissue with non-atherosclerotic intimal thickening using second-harmonic generation imaging [25]. They measured the fiber dispersion and the positive fiber angle with respect to the circumferential axis of the artery in the released, *i.e.* stress-free state, defined here as $\alpha_{rel,\text{exp}}$ and $\kappa_{rel,\text{exp}}$ respectively. They observed a clear distinction between the three arterial layers (intima, media, adventitia), and reported microstructural properties and thickness for each layer. They also quantified the fiber distribution in all layers, which was symmetrical with respect to the circumferential axis. In the same study, mechanical material parameters of the adventitia, media and intima were obtained after fitting a constitutive model to experimental planar biaxial test data. Furthermore, Holzapfel *et al.* reported a layer-specific axial prestretch $g^{(e)}_{ZZ}$ [26]. The median values of all experimental data are shown in Table 1.

To reproduce the transmural distribution of the collagen fiber architecture, the aorta was modeled with an inner radius in the reference state R_{inner} of 10mm, corresponding to a diastolic pressure P_{dias} of 80mmHg [27]. Equation 15 with $\mathbf{F} = \mathbf{I}$ was solved to find the value of $g^{(e)}_{\Theta\Theta,inner}$ for which the computed P matches the desired diastolic pressure P_{dias}. A constant value of 1.1 for the collagen fiber deposition stretch $g^{(c)}$ was used [19]. The cylindrical abdominal aorta, consisting of the intima, media and adventitia is discretized using 5, 25 and 15 integration points throughout each layer respectively. Each layer is modeled using the thicknesses H, mechanical properties C_{10}, k_1, k_2 and layer-specific axial prestretch $g^{(e)}_{ZZ}$ as listed in Table 1. Following equation 14 and given $g^{(e)}_{\Theta\Theta,i=1} = g^{(e)}_{\Theta\Theta,inner}$, $g^{(e)}_{\Theta\Theta}$ for each integration point i throughout the arterial wall is determined as:

$$g^{(e)}_{\Theta\Theta,i} = \frac{R_i}{\sqrt{\left(\frac{R_{i-1}}{g^{(e)}_{\Theta\Theta,i-1}}\right)^2 + g^{(e)}_{ZZ,i-1}(R_i^2 - R_{i-1}^2)}}. \tag{23}$$

The set of nonlinear equations 15 and 18 are solved to find $\lambda_{zz,rel}$ and $\lambda_{\theta\theta,rel,inner}$, characterizing the stress-free state. The values of $g^{(e)}_{\Theta\Theta,inner}$, $\lambda_{\theta\theta,rel,inner}$ and $\lambda_{zz,rel}$ are determined using the nonlinear system solver *fsolve* in Matlab R2019a (The Mathworks Inc., Natick, Massachusetts, USA).

3. Results

The constrained mixture fiber distribution algorithm was tested on an idealized geometry of an abdominal artery. The deposition stretches and corresponding fiber distribution were determined to obtain static equilibrium of the *in vivo* geometry experiencing a known internal pressure, for both a stress- or stretch based fiber distribution method.

The stimuli experienced by the isotropic non-collagenous ECM for both the stress- and stretch-based constrained mixture fiber distribution method are shown on Figures 1 and 2, respectively. The results are shown throughout the arterial wall, *i.e.* radial position, at each integration point (depth of $0\mu m$-$200\mu m$: intima; depth of $200\mu m$-$700\mu m$: media; depth of $700\mu m$-$1000\mu m$: adventitia). The orientations of the first and second principal stress ($k = \sigma$) or stretch ($k = \lambda$) directions $\mathbf{e}_{1,k}^{(e)}$ and $\mathbf{e}_{2,k}^{(e)}$ are shown on top of the graph and can vary between the arterial layers.

The resulting microstructural parameters in the released state, averaged over the integration points of each arterial layer are shown in Table 2. The last column shows the experimental values [25].

The microstructural parameters $\alpha_{0,k}$ and $\kappa_{0,k}$ are used to construct the normalized fiber density $\overline{\rho}(\phi)$ throughout the thickness in the released state, using equation 22. The resulting heatmaps for both algorithms are shown on Figure 3a and Figure 3b, respectively. A representative heatmap of the experimentally observed fiber distribution is shown on Figure 3c (adapted from [25]).

4. Discussion

Our work is driven by the hypothesis that collagen fibers are oriented in an optimal configuration which depends on the external loading of the artery. It has become generally accepted that collagen fibers reorient to maximize the load-bearing capacity of the arterial wall [1, 6, 9]. This rationale is now combined with the constrained mixture theory in which deposition stretches enable static equilibrium in the homeostatic reference configuration under the loads present in this configuration [20]. We assume that fibers are oriented based on the homeostatic stress or stretch experienced by the isotropic non-collagenous ECM in which the collagen fibers are deposited. This is a key difference with previous models [2, 3, 6, 8, 9, 16] where the load or deformation exerted on the entire material determines the fiber orientation. We believe that our approach increases the biofidelity of the fiber distribution algorithm, since the fibroblasts and synthetic smooth muscle cells responsible for synthetizing the fibers are assumed to be embedded in this non-collagenous, isotropic ECM.

Comparison of the stress- and stretch-based constrained mixture fiber distribution algorithms

Considering the lack of consensus whether stretch or stress is the driving factor behind the way fibers are oriented, we implemented both in the framework of the constrained mixture theory and compared their performance. For both methods, we were able to retrieve the diastolic state in which each constituent is related to its respective stress-free state. The variation of the microstructural parameters between the three arterial sublayers, *i.e.* intima, media and adventitia, was larger for the stress-based compared to the stretch-based algorithm, see Table 2, Figures 3a and 3b. We modeled the artery as a cylindrical wall consisting of these arterial layers each with a distinct mechanical behavior, see C_{10}, k_1 and k_2 shown in Table 1. This introduced sharp transitions of the stress-based stimulus functions across the arterial layers, see Figure 1. The first principal stress direction switched from a circumferential orientation in the intima and media towards an axial orientation in the adventitia. On the other hand, the stretch-based stimulus functions did not show similar sharp transitions, because the circumferential stretch, used to define the circumferential deposition stretch corresponding to $s_{1,\lambda}$ in Figure 2, is continuous across the arterial layers. The small difference between the layers can be attributed to the different values for $g^{(e)}_{ZZ}$. Also note that in the

stretch-based case, the first and second principal stretch directions were oriented along the circumferential and axial direction respectively in all arterial sublayers, see Figure 2.

Comparison with experimental data

To validate the implemented algorithms, the results of the proposed methods were compared with experimentally obtained distribution of fibers of a human abdominal aorta. The collagen distribution of this tissue has been extensively studied using various visualization techniques [25, 28, 29]. All studies reported similar results in terms of collagen distribution. This study focuses on [25] because they performed additional layer-specific planar biaxial experiments. As illustrated on Figure 3c, a distinct difference in the structural characteristics between the three arterial sublayers, *i.e.* intima, media and adventitia, was visible. A dispersed structure is observed for the intima layer ($\alpha_{rel,\text{exp}} = 3.25°$ and $\kappa_{rel,\text{exp}} = 0.26$). The media is characterized by two fiber families, more oriented along the circumferential direction ($\alpha_{rel,\text{exp}} = 6.91°$ and $\kappa_{rel,\text{exp}} = 0.21$), while the collagen fibers in the adventitia are more wavy, directed along the axial direction ($\alpha_{rel,\text{exp}} = 77.53°$ and $\kappa_{rel,\text{exp}} = 0.23$). They reported a slightly smaller fiber angle in the media layer compared to [28]. Both the intima-media and media-adventitia are separated by transition layers. Moreover, Niestrawska *et al.* reported a layer-specific out-of-plane dispersion. While this dispersion is an important characteristic of aneurysmatic tissue, little out-of-plane dispersion was observed for healthy abdominal aortic tissue [25]. Accordingly, we decided to omit this when modeling the arterial wall.

The abrupt transitions between the arterial layers of the experimentally observed fiber distribution are more consistent with the results generated by the stress-based fiber distribution method, compared to the stretch-based model (see Figure 3). It is also in line with the conclusion of [7] which stated that stress is the driving factor behind growth and remodeling in arterial tissue. In the remainder of this section, we therefore only focus on the stress-based method when comparing the computed data with the experimental results. Considering the fiber angle in the released state (see Table 2), we were able to qualitatively predict the transitions between the arterial layers. The fiber angle increases radially, starting from a fiber direction close to the circumferential direction in the intima ($\alpha_{rel,\sigma} = 10.67°$), towards a fiber angle which is increasingly oriented towards the axial direction in the media ($\alpha_{rel,\sigma} = 34.99°$) and adventitia ($\alpha_{rel,\sigma} = 54.23°$). Considering the

fiber dispersion (see Table 2), we observed a highly anisotropic intima layer ($\kappa_{rel,\sigma} = 0.06$), while the fibers in the media and adventitia show a higher dispersion value ($\kappa_{rel,\sigma} = 0.22$ and $\kappa_{rel,\sigma} = 0.25$, respectively). To the authors' knowledge, reconstructing an experimental fiber orientation at this scale using a computational algorithm has not been attempted before. Until now, most fiber reorientation algorithms have used the classical modeling framework which requires the knowledge of a stress-free reference state and tissue-level parameters. Using the constrained mixture theory allows for a better physiological comprehension of the fiber distribution. In that respect, we imposed a layer-specific axial prestretch $g^{(e)}_{ZZ}$ obtained from experiments [26] which facilitated a representative reconstruction of a layer-specific fiber distribution. This axial prestretch, representing the overall axial loading, is mainly due to the presence of elastin in the arterial wall [14] and explains why this is assigned to $\mathbf{G}^{(e)}$.

Comparison with other methods

Other reorientation algorithms have successfully predicted the fiber distribution in various tissues such as mitral valves [2, 4], carotid arteries [9, 31], articular cartilage [5] and cornea [32]. The most significant difference between these kind of tissues is the mechanical surrounding environment which dictates the fiber distribution. In the current study, the method has been demonstrated on large, elastic arteries for which its behavior is described using the presented constitutive equations. This method can also be applied on smaller arteries with minor modifications according to their distinctive mechanical environment and their physiology.

It is important to differentiate the presented method from other constrained mixture based growth and remodeling methods. These methods can include implicit mechanisms to account for fiber reorientation by relating the collagen production rate to the loading experienced by the fibers [33]. Other constrained mixture algorithms have explicitly modeled the reorientation of deposited fibers over time [34, 35, 36]. In contrast to these methods, the discussed method determines the fiber distribution in accordance with the deposition stretches that are in equilibrium with the *in vivo* homeostatic reference geometry and the external loading, excluding the long-term remodeling of collagen fibers due to *e.g.* supraphysiological loading conditions.

Limitations and future perspectives

Despite some qualitative similarities of the stress-based algorithm, two clear

differences between the modeled and experimental data are noticeable. First, the intimal fiber dispersion is underestimated. Second, the fiber angle of the media is predicted to be higher compared to the experimental fiber angle. Both differences may be due to the way the fiber distribution is modeled in the intimal layer. In the case study that we considered, which is based on the measurements of [25], we are dealing with a sample with significant non-atherosclerotic intimal thickening. Most collagen fibers in the intimal layer were distributed by the algorithm with a low dispersion in the circumferential direction, accounting for most of the circumferential stress, inducing 'stress shielding' [30]. This effect propagated further in the arterial wall leading to a decrease of the stimulus $s_{1,\sigma}$ and a corresponding increase of the ratio between both stimuli in the media, see Figure 1.

Additionally, blood flow and its interaction with the arterial wall was neglected. It is likely that the blood flow dynamics plays a prominent role on the collagen fiber deposition orientation which is not captured by the proposed method [1]. The corresponding shear stresses are sensed by endothelial cells and may induce remodeling processes affecting the collagen fiber distribution throughout the arterial layers [1]. Further research is therefore necessary to assess the role of the fluid-structure interaction on the collagen fiber distribution of the thickened intimal layer.

All collagen fibers, independent of the arterial sublayer in which they are embedded, were subjected to the same distribution law. Moreover, a constant value of the fiber deposition stretch $g^{(c)}$ has been used, following [20, 21]. However, qualitatively observable differences of the fiber waviness between the arterial layers suggests that $g^{(c)}$ is not constant throughout the arterial layer. Therefore, following [19], having a layer-specific $g^{(c)}$ may lead to a better estimation of the fiber morphology. In addition, the axial prestretch is another important input parameter which needs to be determined *in vitro* [26].

The algorithm is illustrated on an axisymmetric thick-walled cylinder for which the axial, circumferential and radial directions are well-defined and an analytical expression is available to find the deposition stretches and corresponding fiber distributions. However, the applicability of fiber orientation algorithms is defined by their capability to obtain fiber directions for complex geometries with irregular curvatures for which the element-wise circumferential and axial directions are not easily defined. Using the presented method, there is no need to estimate opening angles to account for the residual stresses, omitting the need for a perfect cylindrical model. An important

next step is to investigate the applicability and convergence behavior of the presented constrained mixture fiber distribution methods in patient-specific arteries.

Finally, material parameters were used which were derived from planar biaxial experiments [25]. These parameters were identified using the classical approach, for which the excised, stress-free configuration is defined as the reference state. However, adopting the constrained mixture theory also affects the material parameters. Accordingly, Maes *et al.* developed an iterative fitting approach which generates material properties compatible with the constrained mixture theory [21]. We suggest to expand this fitting method by deriving the fiber distribution, using equations 9, 10 and 11 throughout the iterative fitting process, using the current deposition stretches within each iteration. This effectively reduces the number of parameters to be fitted, since the main fiber directions and dispersion are now fully defined by our algorithm.

5. Conclusion

In this study we introduced a constrained mixture based algorithm which defines the collagen orientation distribution throughout the arterial wall according to the loading experienced by the non-collagenous part of the ECM. We tested both stress- and stretch-driven fiber orientation, applying both approaches on a human abdominal aorta, modeled as a perfect cylinder, and compared with microstructural data from literature. The stretch-based method predicted a fairly uniform fiber distribution throughout the thickness while the stress-based method was able to predict the experimentally observed sharp transitions of the fiber distribution between the arterial sublayers.

Acknowledgements

This work was supported by three doctoral grants from the Research Foundation Flanders (FWO) (SB1SA9119N, 11A6519N, SB1S35316N), a KU Leuven project (C2-ADAPT), and a joined research project between FWO and the Austrian Science Fund (FWF) (G088020N).

References

[1] F. Baaijens, C. Bouten, N. Driessen, Modeling collagen remodeling, Journal of Biomechanics 43 (1) (2010) 166–175. doi:10.1016/j.jbiomech.2009.09.022.

[2] N. J. Driessen, R. A. Boerboom, J. M. Huyghe, C. V. Bouten, F. P. Baaijens, Computational analyses of mechanically induced collagen fiber remodeling in the aortic heart valve, Journal of Biomechanical Engineering 125 (4) (2003) 549–557. doi:10.1115/1.1590361.

[3] N. J. Driessen, W. Wilson, C. V. Bouten, F. P. Baaijens, A computational model for collagen fibre remodelling in the arterial wall, Journal of Theoretical Biology 226 (1) (2004) 53–64. doi:10.1016/j.jtbi.2003.08.004.

[4] N. J. Driessen, C. V. Beuten, F. P. Baaijens, Improved prediction of the collagen fiber architecture in the aortic heart valve, Journal of Biomechanical Engineering 127 (2) (2005) 329–336. doi:10.1115/1.1865187.

[5] W. Wilson, N. J. Driessen, C. C. van Donkelaar, K. Ito, Prediction of collagen orientation in articular cartilage by a collagen remodeling algorithm, Osteoarthritis and Cartilage 14 (11) (2006) 1196–1202. doi:10.1016/j.joca.2006.05.006.

[6] N. J. Driessen, M. A. Cox, C. V. Bouten, F. P. Baaijens, Remodelling of the angular collagen fiber distribution in cardiovascular tissues, Biomechanics and Modeling in Mechanobiology 7 (2) (2008) 93–103. doi:10.1007/s10237-007-0078-x.

[7] L. A. Taber, J. D. Humphrey, Stress-modulated growth, residual stress, and vascular heterogeneity, Journal of Biomechanical Engineering 123 (6) (2001) 528–535. doi:10.1115/1.1412451.

[8] I. Hariton, G. DeBotton, T. C. Gasser, G. A. Holzapfel, Stress-driven collagen fiber remodeling in arterial walls, Biomechanics and Modeling in Mechanobiology 6 (3) (2007) 163–175. doi:10.1007/s10237-006-0049-7.

[9] I. Hariton, G. DeBotton, T. C. Gasser, G. A. Holzapfel, Stress-modulated collagen fiber remodeling in a human carotid bifurcation, Journal of Theoretical Biology 248 (3) (2007) 460–470. doi:10.1016/j.jtbi.2007.05.037.

[10] A. Grillo, G. Wittum, A. Tomic, S. Federico, Remodelling in statistically oriented fibre-reinforced materials and biological tissues, Mathematics and Mechanics of Solids 20 (9) (2015) 1107–1129. doi:10.1177/1081286513515265.

[11] C. J. Cyron, J. D. Humphrey, Preferred fiber orientations in healthy arteries and veins understood from netting analysis, Mathematics and Mechanics of Solids 20 (6) (2015) 680–696. doi:10.1177/1081286514551495.

[12] T. Waffenschmidt, A. Menzel, Extremal states of energy of a double-layered thick-walled tube - application to residually stressed arteries, Journal of the Mechanical Behavior of Biomedical Materials 29 (2014) 635–654. doi:10.1016/j.jmbbm.2013.05.023.

[13] J. D. Humphrey, K. R. Rajagopal, A constrained mixture model for growth and remodeling of soft tissues, Mathematical Models and Methods in Applied Sciences 12 (3) (2002) 407–430. doi:10.1142/S0218202502001714.

[14] L. Cardamone, A. Valentín, J. F. Eberth, J. D. Humphrey, Origin of axial prestretch and residual stress in arteries, Biomechanics and Modeling in Mechanobiology 8 (6) (2009) 431–446. doi:10.1007/s10237-008-0146-x.

[15] N. Qi, H. Gao, R. W. Ogden, N. A. Hill, G. A. Holzapfel, H. C. Han, X. Luo, Investigation of the optimal collagen fibre orientation in human iliac arteries, Journal of the Mechanical Behavior of Biomedical Materials 52 (2015) 108–119. doi:10.1016/j.jmbbm.2015.06.011.

[16] S. Fausten, D. Balzani, J. Schröder, An algorithmic scheme for the automated calculation of fiber orientations in arterial walls, Computational Mechanics 58 (5) (2016) 861–878. doi:10.1007/s00466-016-1321-z.

[17] K. Garikipati, J. E. Olberding, H. Narayanan, E. M. Arruda, K. Grosh, S. Calve, Biological remodelling: Stationary energy, configurational change, internal variables and dissipation, Journal of the Mechanics and Physics of Solids 54 (7) (2006) 1493–1515. doi:10.1016/j.jmps.2005.11.011.

[18] T. C. Gasser, R. W. Ogden, G. Holzapfel, Hyperelastic modelling of arterial layers with distributed collagen fibre orientations, Journal Of The Royal Society Interface 3 (6) (2006) 15–35. doi:10.1098/rsif.2005.0073.

[19] C. Bellini, J. Ferruzzi, S. Roccabianca, E. S. Di Martino, J. D. Humphrey, A microstructurally motivated model of arterial wall mechanics with mechanobiological implications, Annals of Biomedical Engineering 42 (3) (2014) 488–502. doi:10.1007/s10439-013-0928-x.

[20] N. Famaey, J. Vastmans, H. Fehervary, L. Maes, E. Vanderveken, F. Rega, S. J. Mousavi, S. Avril, Numerical simulation of arterial remodeling in pulmonary autografts, ZAMM - Journal of Applied Mathematics and Mechanics / Zeitschrift für Angewandte Mathematik und Mechanik 98 (12) (2018) 2239–2257. doi:https://doi.org/10.1002/zamm.201700351.

[21] L. Maes, H. Fehervary, J. Vastmans, S. J. Mousavi, S. Avril, N. Famaey, Constrained mixture modeling affects material parameter identification from planar biaxial tests, Journal of the Mechanical Behavior of Biomedical Materials 95 (March) (2019) 124–135. doi:10.1016/j.jmbbm.2019.03.029.

[22] C. J. Cyron, R. C. Aydin, J. D. Humphrey, A homogenized constrained mixture (and mechanical analog) model for growth and remodeling of soft tissue, Biomechanics and Modeling in Mechanobiology 15 (6) (2016) 1389–1403. doi:10.1007/s10237-016-0770-9.

[23] S. J. Mousavi, S. Avril, Patient-specific stress analyses in the ascending thoracic aorta using a finite-element implementation of the constrained mixture theory, Biomechanics and Modeling in Mechanobiology 16 (5) (2017) 1765–1777. doi:10.1007/s10237-017-0918-2.

[24] R. W. Ogden, Nonlinear Continuum Mechanics and Modeling the Elasticity of Soft Biological Tissues with a Focus on Artery Walls, Springer International Publishing, Cham, 2017, pp. 83–156. doi:10.1007/978-3-319-41475-1_3.

[25] J. A. Niestrawska, C. Viertler, P. Regitnig, T. U. Cohnert, G. Sommer, G. A. Holzapfel, Microstructure and mechanics of healthy and aneurysmatic abdominal aortas: Experimental analysis and modelling, Journal of the Royal Society Interface 13 (124) (2016). doi:10.1098/rsif.2016.0620.

[26] G. A. Holzapfel, G. Sommer, M. Auer, P. Regitnig, R. W. Ogden, Layer-specific 3D residual deformations of human aortas with non-atherosclerotic intimal thickening, Annals of Biomedical Engineering 35 (4) (2007) 530–545. doi:10.1007/s10439-006-9252-z.

[27] B. Sonesson, F. Hansen, H. Stale, T. Länne, Compliance and diameter in the human abdominal aorta-The influence of age and sex, European Journal of Vascular Surgery 7 (6) (1993) 690–697. doi:10.1016/S0950-821X(05)80718-2.

[28] A. J. Schriefl, G. Zeindlinger, D. M. Pierce, P. Regitnig, G. A. Holzapfel, Determination of the layer-specific distributed collagen fibre orientations in human thoracic and abdominal aortas and common iliac arteries, Journal of the Royal Society Interface 9 (71) (2012) 1275–1286. doi:10.1098/rsif.2011.0727.

[29] A. J. Schriefl, H. Wolinski, P. Regitnig, S. D. Kohlwein, G. A. Holzapfel, An automated approach for three-dimensional quantification of fibrillar structures in optically cleared soft biological tissues, Journal of the Royal Society Interface 10 (80) (2013). doi:10.1098/rsif.2012.0760.

[30] F. Nappi, A. R. Carotenuto, D. Di Vito, C. Spadaccio, C. Acar, M. Fraldi, Stress-shielding, growth and remodeling of pulmonary artery reinforced with copolymer scaffold and transposed into aortic position, Biomechanics and Modeling in Mechanobiology 15 (5) (2016) 1141–1157. doi:10.1007/s10237-015-0749-y.

[31] M. Ghasemi, R. D. Johnston, C. Lally, Development of a Collagen Fibre Remodelling Rupture Risk Metric for Potentially Vulnerable Carotid

Artery Atherosclerotic Plaques, Frontiers in Physiology 12 (October) (2021) 1–17. doi:10.3389/fphys.2021.718470.

[32] D. Zhou, A. Abass, A. Eliasy, A. Movchan, N. Movchan, A. Elsheikh, Numerical simulation of corneal fibril reorientation in response to external loading, International Journal of Environmental Research and Public Health 16 (18) (2019). doi:10.3390/ijerph16183278.

[33] A. Valentín, J. D. Humphrey, G. A. Holzapfel, A finite element-based constrained mixture implementation for arterial growth, remodeling, and adaptation: Theory and numerical verification, International Journal for Numerical Methods in Biomedical Engineering 29 (8) (2013) 822–849. doi:10.1002/CNM.2555.

[34] S. Baek, K. R. Rajagopal, J. D. Humphrey, A theoretical model of enlarging intracranial fusiform aneurysms, Journal of Biomechanical Engineering 128 (1) (2006) 142–149. doi:10.1115/1.2132374.

[35] J. S. Wilson, S. Baek, J. D. Humphrey, Importance of initial aortic properties on the evolving regional anisotropy, stiffness and wall thickness of human abdominal aortic aneurysms, Journal of the Royal Society, Interface 9 (74) (2012) 2047–2058. doi:10.1098/RSIF.2012.0097.

[36] M. Latorre, J. D. Humphrey, Numerical knockouts–In silico assessment of factors predisposing to thoracic aortic aneurysms, PLOS Computational Biology 16 (10) (2020) e1008273. doi:10.1371/JOURNAL.PCBI.1008273.

Tables

Table 1: Median values of the layer-specific thickness, material and microstructural properties of abdominal aortic tissue. The *in vivo* thickness (H), material (C_{10}, k_1, k_2) and microstructural ($\alpha_{rel,\text{exp}}$, $\kappa_{rel,\text{exp}}$) properties are taken from [25]. The axial prestretch $g^{(e)}_{ZZ}$ is taken from [26], after multiplying the *in situ* axial prestretch after excision with the layer-specific axial prestretch after separation. The microstructural properties are given in the released, *i.e.* stress-free, state.

	Intima	Media	Adventitia	Source
H [mm]	0.20	0.50	0.30	[25]
C_{10} [kPa]	16.90	8.00	1.89	[25]
k_1 [kPa]	7.79	11.68	0.36	[25]
k_2 [-]	139.10	7.18	45.88	[25]
$\alpha_{rel,\text{exp}}$ [°]	3.25	6.91	77.53	[25]
$\kappa_{rel,\text{exp}}$ [-]	0.26	0.21	0.23	[25]
$g^{(e)}_{ZZ}$ [-]	1.15	1.24	1.31	[26]

Table 2: The resulting microstructural parameters in the released state, calculated by the stress-based ($k = \sigma$) and stretch-based ($k = \lambda$) reorientation algorithm averaged over the arterial layers (I=intima; M=media; A=adventitia), as well as the experimental values ($k = \exp$) observed by [25]. I=intima; M=media; A=adventitia.

		Stimulus $k = \sigma$	Stimulus $k = \lambda$	Experimental $k = \exp$ [25]
I	$\alpha_{rel,k}[^\circ]$	10.67	40.85	3.25
	$\kappa_{rel,k}[-]$	0.06	0.13	0.26
M	$\alpha_{rel,k}[^\circ]$	34.99	45.74	6.91
	$\kappa_{rel,k}[-]$	0.22	0.18	0.21
A	$\alpha_{rel,k}[^\circ]$	54.23	48.87	77.53
	$\kappa_{rel,k}[-]$	0.25	0.23	0.23

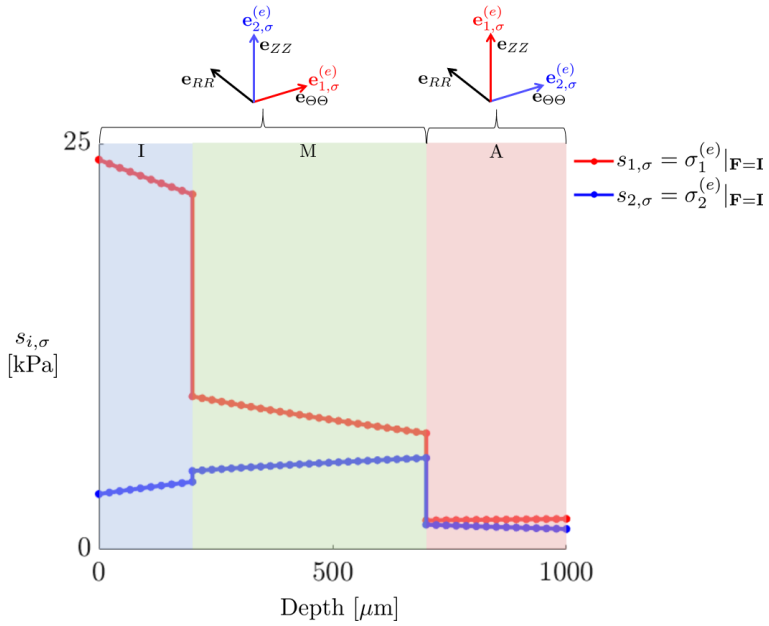

Figure 1: The stimuli experienced by the isotropic non-collagenous ECM for the stress-based constrained mixture reorientation method. The stimulus along the first principal stress direction is shown in red, the stimulus along the second principal stress direction is shown in blue. For each radial position, the first and second principal stress directions are shown in terms of the axial ($\mathbf{e}_{ZZ}$), circumferential ($\mathbf{e}_{\Theta\Theta}$) and radial ($\mathbf{e}_{RR}$) direction. I=intima (shaded blue area); M=media (shaded green area); A=adventitia (shaded red area).

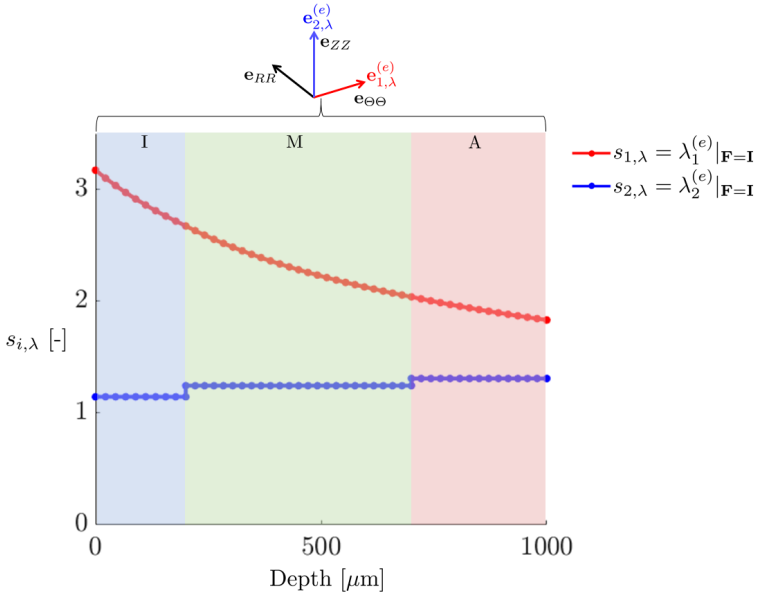

Figure 2: The stimuli experienced by the isotropic non-collagenous ECM for the stretch-based constrained mixture reorientation method. The stimulus along the first principal stretch direction is shown in red, the stimulus along the second principal stretch direction is shown in blue. For each radial position, the first and second principal stretch directions are shown in terms of the axial ($\mathbf{e}_{ZZ}$), circumferential ($\mathbf{e}_{\Theta\Theta}$) and radial ($\mathbf{e}_{RR}$) direction. I=intima (shaded blue area); M=media (shaded green area); A=adventitia (shaded red area).

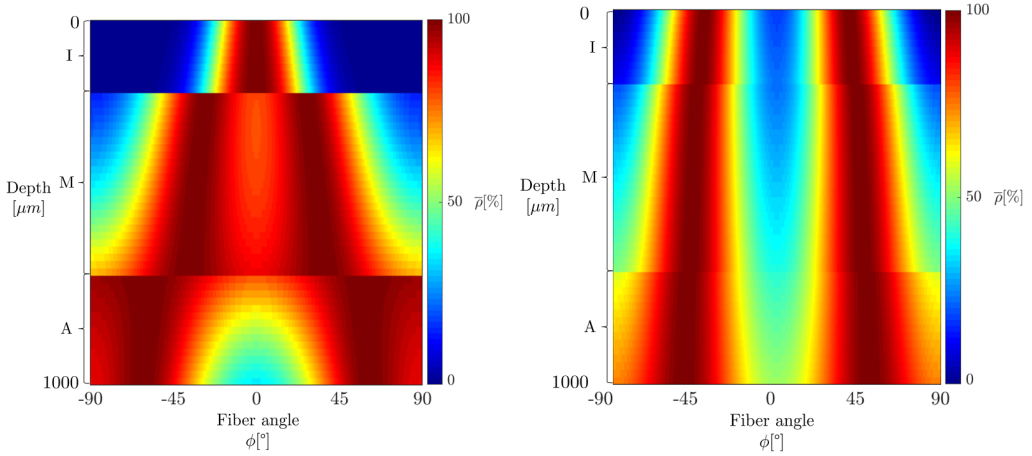

(a) $k = \sigma$

(b) $k = \lambda$

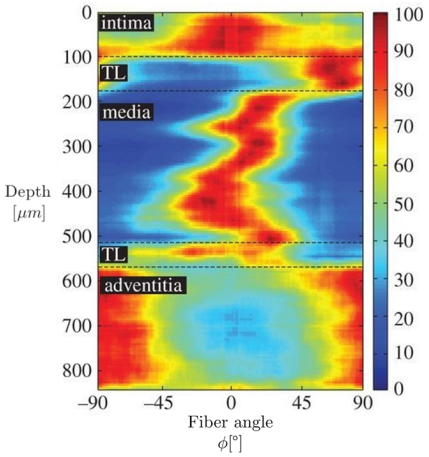

(c) Experimental

Figure 3: Fiber distribution of a healthy human abdominal aorta with non-atherosclerotic intimal thickening in function of the fiber angle ϕ with respect to the circumferential axis in the stress-free state, calculated by the stress-based (3a) and stretch-based 3b constrained mixture based fiber distribution algorithm. I=intima; M=media; A=adventitia. The experimentally observed fiber distribution is illustrated by a representative example (3c, adapted from [25]). A red color indicate a high collagen fiber density, a blue color indicated a low collagen fiber density.